Solution Structure of a Cis-Opened (10*R*)-N^6-Deoxyadenosine Adduct of (9*S*,10*R*)-9,10-Epoxy-7,8,9,10-tetrahydrobenzo[*a*]pyrene in a DNA Duplex[†,‡]

David E. Volk,[§] Varatharasa Thiviyanathan,[§] Jeffrey S. Rice,[§,||] Bruce A. Luxon,[§] Jamshed H. Shah,[⊥] Haruhiko Yagi,[⊥] Jane M. Sayer,[⊥] Herman J. C. Yeh,[⊥] Donald M. Jerina,[⊥] and David G. Gorenstein*[,§]

Sealy Center for Structural Biology and Department of Human Biological Chemistry and Genetics, University of Texas Medical Branch, Galveston, Texas 77555-1157, and Laboratory of Bioorganic Chemistry, National Institute of Diabetes and Digestive and Kidney Diseases, National Institutes of Health, DHHS, Bethesda, Maryland 20892-0820

Received August 27, 2002; Revised Manuscript Received December 13, 2002

ABSTRACT: The solution structure of an 11-mer DNA duplex, d(CGGTCA*CGAGG)·d(CCTCGTGACCG), containing a 10*R* adduct at dA* that corresponds to the cis addition of the N^6-amino group of dA_6 to (+)-(9*S*,10*R*)-9,10-epoxy-7,8,9,10-tetrahydrobenzo[*a*]pyrene was studied by 2D NMR methods. The NOESY cross-peak patterns indicate that the hydrocarbon is intercalated on the 5′-side of the modified base. This observation is the same as that observed for other oligonucleotides containing (10*R*)-dA adducts but opposite to that observed for the corresponding (10*S*)-dA adducts which are intercalated on the 3′-side of the modified base. The hydrocarbon is intercalated from the major groove without significant disruption of either the anti glycosidic torsion angle of the modified residue or the base pairing of the modified residue with the complementary residue on the opposite strand. The ensemble of 10 structures determined exhibits relatively small variations (6−15°) in the characteristic hydrocarbon−base dihedral angles (α′ and β′) as well as the glycosidic torsion angle χ. These angles are similar to those in a previously determined cis-opened benzo[*a*]pyrene diol epoxide-(10*R*)-dA adduct structure. Comparison of the present structure with the cis-opened diol epoxide adduct suggests that the absence of the 7- and 8-hydroxyl groups results in more efficient stacking of the aromatic moiety with the flanking base pairs and deeper insertion of the hydrocarbon into the helix. Relative to normal B-DNA, the duplex containing the present tetrahydroepoxide adduct is unwound at the lesion site, whereas the diol epoxide adduct structure is more tightly wound than normal B-DNA. Buckling of the adducted base pair as well as the C_5-G_{18} base pair that lies immediately above the hydrocarbon is much less severe in the present adducted structure than its cis-opened diol epoxide counterpart.

The environmental pollutant benzo[*a*]pyrene (BP),[1] one of the best studied carcinogenic agents, is metabolized in mammals to form highly reactive, carcinogenic benzo-ring 7,8-diol 9,10-epoxides (DEs) in which the epoxide group is located in a bay region of the molecule (*1*). These epoxides form covalent adducts with cellular DNA via cis or trans epoxide ring opening by the exocyclic N^2- and N^6-amino groups of deoxyguanosine (dG) and deoxyadenosine (dA), respectively (*2*) (cf. Figure 1). Incorrect replication of such damaged DNA results in mutations and thus likely constitutes the initiating event in cell transformation leading to cancer induced by the DEs. The solution conformations of such adducts in DNA are thus of considerable interest.

We are interested in the effect of the 7- and 8-hydroxyl groups on the physical properties and biological activity of BP DEs and their DNA adducts. Replacement of these hydroxyl groups in BP DE with hydrogen markedly enhances the reactivity of the resulting 9,10-epoxy-7,8,9,10-tetrahydrobenzo[*a*]pyrene (BP H_4E) toward epoxide ring opening by solvent water (*3*), an effect which was ascribed in large part to a greater preference of the BP H_4E (relative to the DEs) for a conformation favoring formation of the carbocation intermediate at C-10. BP H_4E reacts with the exocyclic amino groups of both dG and dA residues to form adducts with DNA in vitro (*4*) as do the BP DEs. Oligonucleotide duplexes containing BP H_4E-dA adducts exhibit decreased thermal denaturation (T_m) temperatures relative to the unadducted duplexes; for example, the present *cis*-(10*R*)-BP H_4E adducted duplex and its cis 10*S* diastereomer have T_m values that are 9 and 14 °C lower than the corresponding unmodified duplex (*5*). Similar trends have been observed

[†] This research was supported by NIH (ES06839 and 1P30 ES06676), Welch Foundation (H-1296), and Sealy and Smith Foundation grants to D.G.G. Building funds were provided by the NIH (1CO6CA59098).

[‡] The structures and constraints have been deposited in the RCSB Protein Data Bank (1N8C).

* Address correspondence to this author. Tel: 409-747-6800. Fax: 409-747-6850. E-mail: david@nmr.utmb.edu.

[§] University of Texas Medical Branch.

[||] Present address: Soldier Biological and Chemical Command Army, Aberdeen Proving Ground, MD 21010-5424.

[⊥] National Institute of Diabetes and Digestive and Kidney Diseases, National Institutes of Health.

[1] Abbreviations: BP, benzo[*a*]pyrene; BP DE, 7,8-dihydroxy-9,10-epoxy-7,8,9,10-tetrahydrobenzo[*a*]pyrene (BP DE-1 and DE-2, isomers in which the benzylic 7-hydroxyl group and the epoxide oxygen are cis and trans, respectively); BP H_4E, 9,10-epoxy-7,8,9,10-tetrahydrobenzo[*a*]pyrene; NOESY, nuclear Overhauser effect spectroscopy; r-MD, restrained molecular dynamics; MORASS, multiple Overhauser relaxation analysis and simulation; PME, particle mesh Ewald.

10.1021/bi026745u CCC: $25.00
Published on Web 01/22/2003

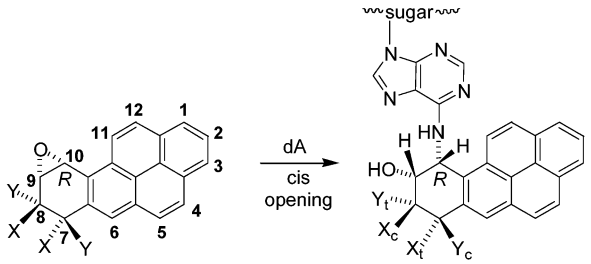

5′-C_1 G_2 G_3 T_4 C_5 **A_6*** C_7 G_8 A_9 $G_{10}G_{11}$-3′
3′-$G_{22}C_{21}C_{20}A_{19}G_{18}T_{17}$ $G_{16}C_{15}T_{14}C_{13}C_{12}$-5′

FIGURE 1: Structures and numbering convention for the BP DEs and BP H_4E and the products of their cis opening at C10 by the exocyclic N^6-amino group of dA in DNA. For each structure, only the enantiomer with 10*R* configuration and the resultant cis-opened (10*R*)-dA adduct diastereomer (BP H_4E dA adduct isomer used in this study) are shown. The subscripts c and t, as used in the text to identify protons cis and trans, respectively, to the proton at C10 of the present BP H_4E adduct, are indicated on the adduct structure. Since the adducts arise by cis attack at C10, the configuration at this carbon is retained upon adduct formation. The modified oligonucleotide duplex is shown with the adduct indicated as A*.

for trans-opened BP DE-dA adducts (reviewed in ref *5*). Metabolism of 7,8-dihydro-BP by mammalian cytochromes P450 produces BP H_4E, with the (+)-(9*S*,10*R*)-enantiomer predominating (*6*−*8*). Racemic BP H_4E exhibits generally higher mutagenicity than the corresponding racemic BP DEs in several strains of *Salmonella typhimurium* but lower mutagenicity than the DEs in Chinese hamster V79 cells (*9*). In a site-specific mutagenesis study (*10*) of BP-derived dA adducts in *Escherichia coli*, decreasing the number of adduct hydroxyl groups generally decreased the total frequency of substitution mutations induced. Interestingly, however, the (9*S*,10*R*)-dA adduct corresponding to cis opening of (+)-(9*S*,10*R*)-BP H_4E constituted a striking exception, in that it exhibited the highest mutational frequency of all the BP dA adducts studied, including the DE adducts (*10*). This 10*R* adduct is the subject of the present study.

Solution structures of duplex oligonucleotides containing both cis- (*11*) and trans- (*12*−*15*) opened (10*R*)-dA adducts derived from BP DEs have been determined by two-dimensional NMR studies. Both cis- and trans-opened dA adducts with this *R*-configuration at the point of attachment of the adenine base have the aromatic hydrocarbon intercalated into the DNA and oriented on the 5′-side of the modified adenine. In the present study we have determined the solution conformation of the cis-opened (9*S*,10*R*)-dA adduct derived from (+)-(9*S*,10*R*)-BP H_4E and compared it to related DE adducts in order to explore the effect of replacing the 7- and 8-hydroxyl groups with hydrogen on the conformation of an 11-mer oligonucleotide duplex (Figure 1) containing this adduct.

MATERIALS AND METHODS

Synthesis of Oligonucleotides. Synthesis of the diastereomeric mixture (10*R*/10*S*) of *cis*-N^6-(10-(9-acetoxy-7,8,9,-10-tetrahydrobenzo[*a*]pyrenyl))-5′- *O*-(4,4′-dimethoxytrityl)-3′-*O*-[(*N*,*N*-diisopropylamino)(β-cyanoethoxy)phosphinyl]-2′-deoxyadenosine and preparation of oligonucleotides used essentially the methodology described (*16*) for the corresponding trans-adducted phosphoramidite (see Supporting Information). The *cis*-phosphoramidite mixture was used to prepare the diastereomeric pair of oligonucleotides corresponding to cis-opened dA adducts of (±)-9,10-epoxy-7,8,9,-10-tetrahydrobenzo[*a*]pyrene by a semiautomated procedure (*17*) with manual coupling of the phosphoramidite. For a 10 μmol synthesis, 130 mg of 170 Å dG-cpg (77 μmol/g) was used. After automated synthesis of a 5-mer corresponding to the 3′-sequence, the support-bound oligonucleotide was treated with 29 μmol of the phosphoramidite in 200 μL of 0.5 M 1*H*-tetrazole in CH_3CN for 18 h at room temperature. Because of potential loss of the 5′-dimethoxytrityl protecting group during the extended coupling time, end capping was omitted following the manual coupling step (*18*). End capping is unnecessary after this step, since failure to couple the adducted phosphoramidite would result in a shorter oligonucleotide lacking the hydrocarbon, which is easily separated from the desired, adducted products by HPLC. The yield of the manual coupling step estimated from the release of the dimethoxytrityl cation (498 nm) was approximately 66%. This coupling yield was significantly higher than those normally observed with the corresponding O-acetylated DE-adducted dA phosphoramidites, possibly due to decreased steric hindrance by substituents on the tetrahydro ring. The final five residues were added by automated synthesis. The fully deprotected oligonucleotides were purified by HPLC on a Hamilton PRP-1 column, 21.5 × 150 mm, eluted at 9 mL/min with a linear gradient of CH_3CN in 0.1 M $(NH_4)_2CO_3$, pH 7.5, that increased the CH_3CN composition from 10% to 30% over 20 min, with detection at 350 nm. The two diastereomeric, adducted oligonucleotides are well separated from each other, with retention times of 10.0 and 11.9 min. Their absolute configurations were assigned on the basis of their CD spectra (see Supporting Information), which exhibited strong positive bands in the 300−360 nm region for the 10*R* (early-eluting) and strong negative bands for the 10*S* (late-eluting) diastereomer, as previously observed for oligonucleotides containing BP DE-dA adducts (*19*). The adducted 11-mers were titrated spectrophotometrically (353 nm) with the complementary strand, d(CCTCGTGACCG), at 20 °C (10*S* isomer) or 25 °C (10*R* isomer) as described (*20*) to determine the amount required to obtain a 1:1 duplex. A ratio of 0.71 A_{260} of complementary strand to 1.0 A_{260} of adducted strand was obtained for both diastereomers. For NMR studies, the 10*R* adducted oligonucleotide was dissolved in 20 mM sodium phosphate buffer, pH 7, containing 57 mM NaCl (to give a total ionic strength of 100 mM) and 0.5 mM sodium azide.

An attempt to investigate the 10*S*-adducted duplex by NMR failed as a result of substantial decomposition of the duplex oligonucleotide in the above sodium phosphate buffer (pH 6.7−7.0) to give 9,10-dihydroxy-7,8,9,10-tetrahydrobenzo[*a*]pyrene: *m*/*z* (FAB MS) 288 ($M^+ + 1$). This decomposition product was cochromatographic with the authentic *trans*-diol obtained on hydrolysis of BP H_4E. Notably, storage of the adducted duplex in buffer at 2 °C produced little or no decomposition after 8 days. However, significant (∼20%) decomposition was observed on HPLC after further storage at room temperature for 6 days, with concomitant formation of an oligonucleotide product lacking the hydrocarbon chromophore. This new oligonucleotide was chro-

matographically distinct (earlier eluting) from the complementary strand and presumably corresponds to the 11-mer with a normal dA at position 6 that is generated upon loss of the hydrocarbon moiety.

NMR Experiments. All NMR spectra were collected on Varian UNITYplus 750 or 600 spectrometers equipped with pulsed field gradients. Samples for the NMR experiments were prepared in a buffer containing 20 mM sodium phosphate (pH 6.7), 56 mM NaCl, and 50 μM sodium azide. For nonexchangeable protons, two-dimensional NOESY data were collected with the sample dissolved in 99.96% D_2O. The data were collected at 750 MHz, using the WETNOESY pulse sequence (*21*) and 200 ms mixing time, at 15 °C with 4096 complex points in t_2 and 512 complex points in t_1, sweep widths of 7455.7 Hz in both dimensions, and a relaxation delay of 4.3 s. The 200 ms mixing time NOESY at 600 MHz was carried out at 5 °C in 90% H_2O/10% D_2O with 8192 complex points in t_2 and 512 complex points in t_1, sweep widths of 12000 Hz, and a relaxation delay of 3.8 s. The Z-filtered TOCSY (*22*) experiments were recorded with 50 and 120 ms mixing times. ROESY (*23*) and exchange-only experiments (*24*) were recorded with 200 and 150 ms mixing times, respectively. All NMR data were processed using VNMR (Varian) software. A 90° shifted sine-bell apodization function was applied to the fids in both dimensions of the NOESY experiments before Fourier transformation.

Creation of AMBER Force Field Parameters and the Starting Structure. Equilibrium bond lengths, bond angles, and dihedral angles for the BP moiety were obtained from a Gaussian94 (*25*) geometry optimization of the BP-adducted dA residue using the 6-31g(d) basis set at the RHF level of theory. Population analysis was calculated in a subsequent Gaussian94 run with the following options: GEOM = ALLCHECK, POP = MK, and IOP(6/33 = 2). A two-part RESP procedure was then used to calculate the final charges for the force field. To create the starting model, NAB (Nucleic Acid Builder; *26*) was used to create the B-DNA form of the duplex without the adduct. The name of residue A^*_6 was edited in the PDB file to residue THB. After the newly created force field parameters were loaded into the xLEAP program within AMBER5.0 (*27*), the altered PDB file was loaded and xLEAP added the missing BP moiety to the duplex. MIDAS was then used to rotate bond angles at the adduct and the surrounding bases to remove all steric clashes while leaving the BP moiety partially intercalated within the helix. This was accomplished by incrementally rotating the A^*_6 H1′−C1′−N9−C8 dihedral angle from −161° to −172°, and the A^*_6/BP H61−N^6−C10−H10 dihedral angle to 150°, while making subtle changes to the neighboring residues and subsequently minimizing the structure to relieve steric clashes with neighboring bases.

Restrained Molecular Dynamics Calculations. These starting model coordinates, based on standard B-DNA with anti glycosidic angles for all residues including the adducted deoxyadenosine, were subjected to energy minimization to remove any unfavorable van der Waals contacts. The starting structure was then placed in a rectangular box, providing at least 10 Å of explicit TIP3P water molecules (*28*). To neutralize the negative charges on phosphates, 22 Na^+ ions were placed around the phosphate groups of the DNA backbone. The water box was first subjected to a series of equilibration MD runs while the solute was held fixed. Position constraints on solute molecules were gradually relaxed during the equilibration steps. These steps were performed using the PME method to calculate electrostatic interactions (*29*). The resulting structure was used as the starting structure for the subsequent rounds of refinement using r-MD. During r-MD, the nonbonded interaction cutoff distance was set to 10 Å with an integration time step of 1 fs. Coordinates were stored every 100 steps. The charges at the 5′- and 3′-ends of the DNA strands were modified to avoid nonphysical electrostatic interactions.

Distance restraints between nonexchangeable protons were derived from the integrated 2D NOESY cross-peak volumes using the hybrid, complete relaxation matrix program MORASS (*30*). Two-dimensional NOESY spectra were simulated from starting model structures at 200 ms mixing time assuming an isotropic correlation time of 4.0 ns. A hybrid of experimentally determined NOESY cross-peak volumes and calculated NOESY volume matrix of starting geometry was built to approximate a complete experimental NOESY volume matrix. The cross-relaxation rate for each proton pair was then calculated with multiple spin effects explicitly treated. Interproton distances were calculated from the cross-relaxation rates assuming a simple isotropic spectral density function.

Using MORASS, 464 distance restraints between nonexchangeable protons were obtained from the 2D NOESY data. In addition, 65 distance restraints between exchangeable protons were obtained by qualitatively measuring the intensities of NOESY cross-peaks from a 90% H_2O/10% D_2O NOESY spectrum at 750 MHz. These restraints were assigned as strong (1.80− 2.50 Å), medium (1.80−3.80 Å), weak (1.80−5.00 Å), and very weak (1.80−6.00 Å). Hydrogen bond restraints at an equilibrium distance of 1.9 Å (±0.19 Å) were added between the base pairs. The force constant on each hydrogen bond restraint was 15 kcal/(mol·$Å^2$). Only one hydrogen bond restraint was applied to either AT (between N1 of A and H3 of T) or GC base pairs (between H1 of G and N3 of C) to allow propeller twist between the base pairs during the refinement.

The structure refinement was done by an iterative cycle involving a perturbational merging of experimental NOESY volumes with the theoretical volume matrix using the MORASS/AMBER protocol as previously described (*15*). In the initial rounds of the iterative r-MD cycles (rounds 1−5), 464 nonexchangeable and 11 hydrogen bond distance restraints were used. For each iteration, the starting structure was subjected to 8 ps of r-MD with temperature annealing (increased the temperature from 298 to 600 K for 2 ps, cooled to 298 K over the next 3 ps, continued at 298 K for the last 3 ps). The average structure from the last 3 ps of the r-MD was energy minimized (2000 steps without restraints), and the resulting structure was used as the starting structure for the next iteration of MORASS/r-MD. For the last iterative cycle of the 8 ps r-MD, an additional 65 distance restraints between exchangeable protons and 86 backbone dihedral angle restraints were also used. The coordinates from the last picosecond of the r-MD calculations were averaged using CARNAL (*31*), and the averaged coordinate set was refined by 2000 steps of full conjugate gradient minimization without NOESY restraints to yield the final averaged structure for each cycle.

The progress of the iterative refinement process was monitored by the % RMS (volume), the *R*-factor, and the $Q^{1/6}$-factor. These factors, defined below, indicate the match between the experimental and theoretical NOESY volumes calculated from the refined structure. The % RMS (volume) is given by

$$\%\ \text{RMS (volume)} = \sqrt{1/N\sum_{ij}\left(\frac{v_{ij}^{a} - v_{ij}^{b}}{v_{ij}^{a}}\right)^2} \times 100$$

The *R*-factor is given by

$$R = \frac{\sum_{ij}|v_{ij}^{a} - v_{ij}^{b}|}{\sum_{ij}v_{ij}^{a}}$$

and the $Q^{1/6}$-factor is defined as

$$Q^{1/6} = \frac{\sum_{ij}\tau_{\mathrm{m}}|(v_{ij}^{a})^{1/6} - (v_{ij}^{b})^{1/6}|}{\sum_{ij}(1/2)\tau_{\mathrm{m}}|(v_{ij}^{a})^{1/6} + (v_{ij}^{b})^{1/6}|}$$

where *a* represents theoretical volumes and *b* represents experimental volumes and τ_{m} is the NOESY mixing time.

To study the conformational space of the adducted duplex, the structure from the last round (round 6) of the MORASS/r-MD iterative cycles was subjected to a further 50 ps of restrained molecular dynamics. The first 10 ps were discarded, and the structure was sampled every 4 ps. These 10 structures were then minimized without restraints. The final restraint penalties for the 10 structures ranged from 40 to 80 kcal/mol. All structures were built with xLEAP (*32*) and displayed with MolMol or MIDAS (*33*). For energy comparisons with the initial structure, the final 10 structures were also minimized with 2000 steps of full conjugate gradient minimization in the absence of water so that the energy of the DNA duplex was not buried within the much larger energies of the solvent system.

RESULTS

Assignments of Nonexchangeable Proton Chemical Shifts. The chemical shift assignments were made using the 2D NOESY, TOCSY, and the DQF-COSY experiments following the established sequential assignment strategy for nucleic acids (*34*). Although neither an A-form nor B-form type geometry was assumed, the sequential assignment of this duplex followed that for a right-handed helix. Sequential assignments were based on the aromatic−H1′ connectivities (Figure 2) and were confirmed by the aromatic−aromatic cross-peaks and aromatic−H2′/H2″/H3′ connectivities. The adenine H2 resonances were assigned by their strong cross-strand NOESY cross-peaks to base-paired thymidine imino protons and by their sequential NOESY cross-peaks to the H1′ of the 3′-residue. Weak sequential H1′(*n*) → H1′(*n* + 1) connectivities were also observed and were used to confirm the H1′ assignments. Sugar H2′ and H2″ resonances were assigned by comparing the intensities of intrasugar NOEs at short mixing times. The sugar H2′ proton is closer to the H1′ of the same sugar than any other proton irrespective of the sugar pucker. Other sugar protons were assigned from the 2D TOCSY and the DQF-COSY spectra.

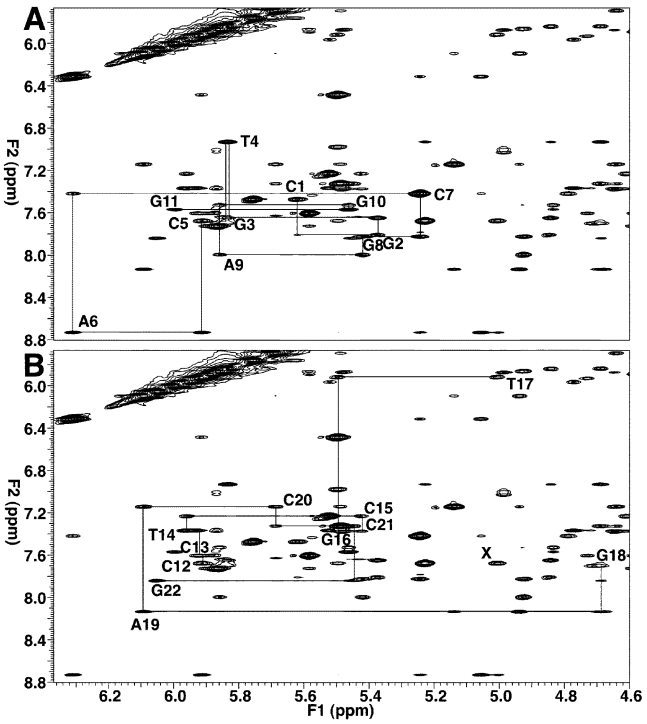

FIGURE 2: The aromatic (F_1) and H1′ (F_2) proton region of a 200 ms mixing time NOESY experiment of the 11-mer duplex in D_2O. (A) Sequential connectivity between the base aromatic and the H1′ protons of the adducted strand. (B) Sequential connectivity of the complementary strand. The sequential connectivity between T_{17} H1′ and G_{18} H8 is not seen. The peak marked with an X is the cross-peak between the C_5 H6 proton and its own H3′ proton.

The assignments of individual sugar protons were confirmed by the relative intensities of the intrasugar cross-peaks in the 2D NOESY spectra.

The chemical shift assignments for the DNA protons are listed in Table 1. Several of the resonances for T_{17} and G_{18} residues are shifted upfield from their normal regions. These include the H1′ protons of T_{17} and G_{18} and the methyl protons of T_{17} as well as the imino protons of T_{17} and G_{18} residues. In contrast, the A^*_6 H8 base proton resonates downfield relative to a normal adenine H8 proton. These changes in chemical shift can be attributed to electron shielding or deshielding effects of the aromatic hydrocarbon. Sequential aromatic−H1′ NOE connectivities were observed for all residues throughout the strand except between G_{18} and T_{17}. This is due to the wedge created by the intercalated BP between these two residues.

Benzo[a]pyrene Protons. The protons of the hydrocarbon were assigned from the 2D TOCSY and NOESY data and comparison with previous BP DE-adducted DNA duplexes (*11*, *15*). The chemical shifts of the BP protons are listed in Table 2. The structure, labeling convention, and absolute configuration for the BP (10*R*)-dA adduct are shown in Figure 1. The TOCSY spectra established the through-bond connectivities for aromatic and aliphatic protons and identified the spin systems. The NOESY data provided additional through-space connectivities between the adjacent spin systems (between H1 and H12, H3 and H4, H5 and H6, H6 and H7, and H10 and H11). The H11 and H12 protons were readily assigned by their relatively upfield-shifted resonances, possibly due to shielding by surrounding bases, as observed

Table 1: Chemical Shift Assignments (in ppm) of the DNA Protons

residue	H1′	H2′	H2″	H3′	H4′	H5′ [a]	H5″ [a]	H6/8	H2/5/Me	NH(2)
dC_1	5.62	1.75	2.25	4.57	3.94	3.59		7.47	5.75	8.10, 7.04
dG_2	5.38	2.58	2.58	4.85	4.17	3.95	3.84	7.80		13.03
dG_3	5.84	2.42	2.55	4.84	4.29	4.00	4.06	7.65		12.59
dT_4	5.84	1.60	1.99	4.69	3.99	4.07	3.94	6.93	1.04	13.35
dC_5	5.91	2.50	2.64	5.00	4.25	3.97	3.93	7.67	5.23	6.64, 6.10
dA^*_6	6.31	2.67	2.80	5.06	4.46	4.12	4.14	8.73	7.79	6.60
dC_7	5.24	2.11	2.24	4.79	4.10	4.02	4.05	7.42	5.24	8.03, 6.52
dG_8	5.42	2.61	2.68	4.92	4.24	4.01	3.93	7.83		12.87
dA_9	5.86	2.52	2.72	4.93	4.28	4.01	4.07	8.00	7.63	
dG_{10}	5.46	2.38	2.52	4.83	4.21	4.04	4.07	7.53		12.88
dG_{11}	6.00	2.30	2.22	4.48	4.09	3.98	4.03	7.57		
dC_{12}	5.89	2.16	2.47	4.59	4.04	3.69		7.73	5.86	
dC_{13}	5.92	2.11	2.42	4.73	4.11	4.01	4.00	7.61	5.58	8.32, 7.02
dT_{14}	5.97	2.11	2.40	4.77	4.11	4.01		7.37	1.54	13.82
dC_{15}	5.42	1.63	2.00	4.61	3.92	4.01	3.92	7.23	5.52	8.44, 6.99
dG_{16}	5.48	1.97	1.97	4.64	4.05	3.78	3.84	7.38		12.76
dT_{17}	4.99	1.57	1.86	4.54	3.79	3.79		5.87	0.18	11.49
dG_{18}	4.68	2.58	2.58	4.73	4.20	4.12	3.89	7.70		10.86
dA_{19}	6.09	2.66	2.75	4.94	4.36	4.08	4.02	8.13	7.63	
dC_{20}	5.69	1.81	2.23	4.64	4.16	4.02		7.14	5.14	7.89, 6.38
dC_{21}	5.45	1.86	2.20	4.69	3.96	4.02	3.92	7.32	5.49	8.50, 6.94
dG_{22}	6.05	2.52	2.25	4.57	4.07	3.95		7.94		

[a] H5′ and H5″ were not stereospecifically assigned.

Table 2: BP Proton Chemical Shifts

proton	δ (ppm)	proton	δ (ppm)
H1	7.03	$H7_c$ [a]	3.24
H2	7.00	$H8_t$ [a]	2.04
H3	7.35	$H8_c$ [a]	1.92
H4	7.57	H9	4.18
H5	7.59	H10	5.50
H6	7.68	H11	6.48
$H7_t$ [a]	3.08	H12	6.98

[a] Subscripts c and t correspond to cis and trans orientation relative to the proton at C10; see Figure 1.

in previous studies. The NOESY cross-peak between H11 and H10 provided a connection to the aliphatic portion of the hydrocarbon. Sequential NOE peaks were then used to assign the remaining BP aliphatic protons. Intense NOE cross-peaks from the aliphatic H7 protons to a resonance at 7.68 ppm were used to assign the H6 proton. A NOESY cross-peak was also observed between the H6 and H5 protons. Stereospecific assignments of the H7 and H8 protons were determined from the relative intensities of the NOESY cross-peaks and by the TOCSY peaks. Fifty-eight NOESY cross-peaks were observed between BP and DNA protons, 44 of which were to nonexchangeable DNA protons. These cross-peaks are listed in Table 3.

Assignment of Exchangeable Protons. The exchangeable protons were assigned from a 2D NOESY spectrum taken in a 90% H_2O/10% D_2O buffer solution. Both imino proton to imino proton NOE cross-peaks and imino proton to adenine H2 proton NOE cross-peaks were used to assign the imino protons (Table 1). Thymidine imino protons were identified by strong NOESY cross-peaks to the H2 protons of the base-paired adenines. The imino protons were sequentially assigned by tracing through the imino−imino cross-peak connectivity (Figure 3). Due to the intercalation of the hydrocarbon between the A^*_6-T_{17} and C_5-G_{18} base pairs, a sequential NOE was not observed between the T_{17} and G_{18} imino protons. An NOE was observed between the 10.86 ppm resonance and a resonance at 13.35 ppm. The resonance at 13.35 ppm showed a very large NOE cross-peak to a resonance at 7.63 ppm, which corresponds to the H2 proton of dA_{19}. On the basis of this, the resonance at 10.86 was assigned to the G_{18} imino proton, and the

Table 3: Interactions Observed between BP Protons and Other Protons in the DNA Duplex[a]

BP proton	DNA base	DNA proton	BP proton	DNA base	DNA proton
H1	T17	H6	$H8_c$	C5	H5
H1	T17	H1′	$H8_c$	A*6	NH_2
H1	T17	H3′	$H8_c$	T17	NH
H1	T17	H2′			
H1	T17	H2″	H9	C5	H5
H1	G18	H5′	H9	A*6	NH_2
H1	G18	H1′	H9	T17	NH
H1	G18	H4′	H9	G18	H1
H1	G18	H5″			
H1	G18	H2′	H10	C5	H5
			H10	C5	H6
H2	T17	H6	H10	C5	H2′
H2	T17	H1′	H10	A*6	NH_2
H2	T17	H3′	H10	T17	NH
H2	T17	H2′	H10	G18	H1
H2	T17	H2″			
H2	G18	H1′	H11	C5	H2′
H2	G18	H2′	H11	C5	H2″
H2	G18	H4′	H11	C5	H3′
H2	G18	H5′	H11	C5	H5
H2	G18	H5″	H11	C5	H6
			H11	A*6	H2
H5	T17	CH_3	H11	A*6	NH_2
			H11	A*6	H8
H6	T17	CH_3	H11	T17	NH
$H7_t$	C5	H5	H12	A*6	NH_2
$H7_t$	A*6	NH_2	H12	T17	H1′
			H12	T17	NH
$H7_c$	C5	H5	H12	T17	H3′
$H7_c$	A*6	NH_2	H12	G18	H1
			H12	G18	H1′
$H8_t$	A*6	NH_2	H12	G18	H5′
$H8_t$	T17	NH	H12	G18	H5″

[a] Subscripts c and t correspond to cis and trans orientation relative to the proton at C10; see Figure 1.

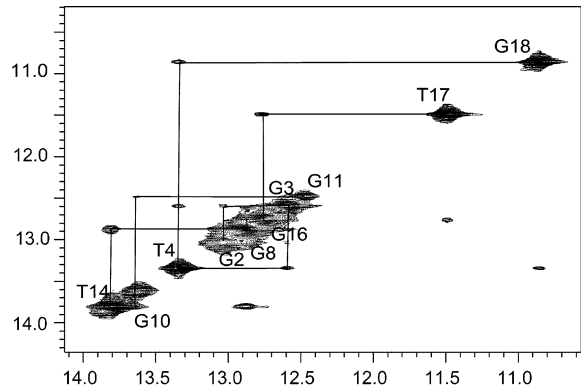

FIGURE 3: Imino−imino cross-peak region of the 2D NOESY spectra collected in H_2O. Base pair to base pair connectivity can be traced from G_2-C_{21} to C_5-G_{18} and then from A^*_6-T_{17} to G_{11}-C_{12}. The break between C_5-G_{18} and A^*_6-T_{17} corresponds to the intercalation site of the hydrocarbon.

resonance at 11.49 ppm was assigned to the T_{17} imino proton. The imino protons of T_{17} and G_{18} showed NOESY cross-peaks to protons on the hydrocarbon (Table 3). The cytidine amino protons were assigned on the basis of the NOEs to the H5 proton, as well as from the NOEs with sequential or cross-strand imino protons. The lone A^*_6 amino proton (on the nitrogen attached to the BP) was determined by a strong NOE to the T_{17} imino proton and the NOEs with hydrocarbon protons near the site of attachment. The imino proton of G_{11} gives a very weak resonance at 12.47 ppm, probably due to the dynamics caused by the end fraying. The imino protons of T_{17} and G_{18} resonate considerably upfield compared to the other imino protons. Upfield-shifted imino resonances usually indicate that the imino protons are only partially hydrogen bonded. However, these two peaks are narrow and intense, indicating that these imino protons are protected by hydrogen bonds and that there is little or no dynamics. Therefore, the upfield shifts of these imino protons are probably due to ring current effects caused by the hydrocarbon moiety that is intercalated between these two residues (Figure 4). Furthermore, the T_{17} imino proton gives NOESY cross-peaks to the A^*_6−H2 and G_{16} imino proton indicating base pairing with A^*_6.

Evidence for 5′-Direction of Intercalation for the Hydrocarbon from DNA to BP NOEs. The abundance of NOESY cross-peaks between BP protons and the DNA bases indicates that the hydrocarbon is stacked in the helix. The ring current effect caused by the intercalated BP moiety causes the H6, methyl, and imino protons of T_{17}, as well as the imino protons of G_{18} and T_{17}, to resonate upfield (Figure 4). The orientation of the hydrocarbon was provided by the NOESY cross-peaks between the protons on the hydrocarbon and the protons in the adjacent DNA residues. Among the total of 58 NOEs observed between protons on the BP moiety and DNA protons, 12 NOEs were between the BP and residue C_5, which is 5′ to the adducted A^*_6 (Table 3). Specifically, interactions between the H5 and/or H6 protons of C_5 and the BP H7, H8, H9, H10, and H11 protons were observed. Additional interactions between the BP H10 and H11 protons with C_5 ribose protons were present. NOE interactions between the BP and T_{17} (20 NOEs), the base across the helix from the adducted A^*_6, and to G_{18} (16 NOEs), the base across the helix from C_5, are also consistent with the 5′-intercalation of the BP. Most of these interstrand NOEs involve the BP

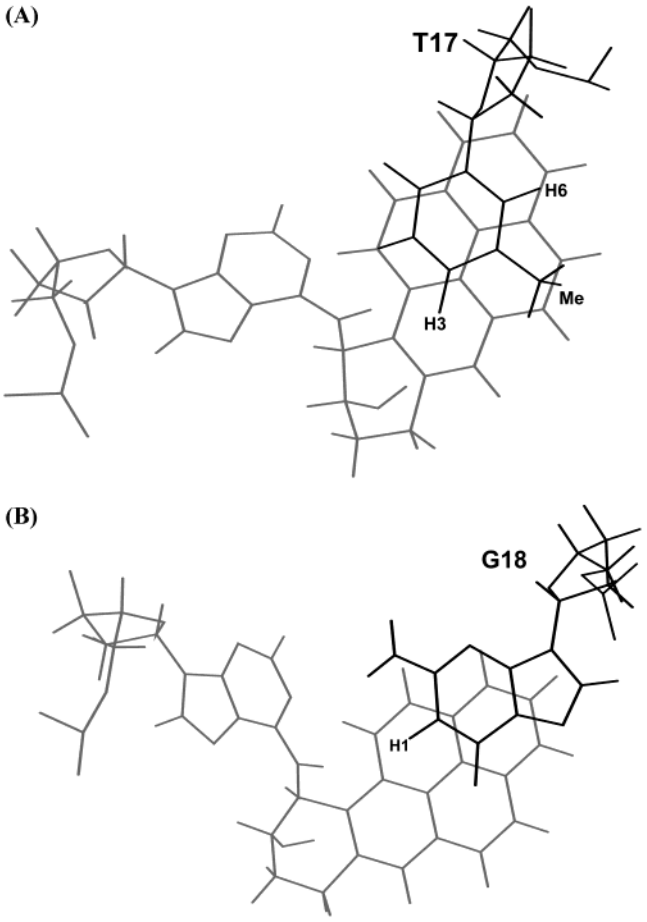

FIGURE 4: Refined structure of the 11-mer duplex with the cis-opened (10*R*)-BP H_4E-dA adduct, viewed along the helical axis. The figure shows the intercalated adduct and the resulting ring current effect on the T_{17} and G_{18} residues. (A) The structure shows the T_{17} methyl (Me) and H6 and H3 imino protons stacked under the hydrocarbon ring, resulting in large upfield chemical shifts. (B) The structure shows the H1 imino proton of G_{18} stacking under the hydrocarbon ring.

H1, H2, and H12 protons of the BP and the ribose protons of residues T_{17} and G_{18}.

Structure Refinement. The progress of the iterative MORASS/r-MD structural refinement, started from a B-DNA model with the hydrocarbon intercalated and anti glycosidic torsional angles for all residues, is shown in Table 4. The % RMS (volume) starts at a relatively high number and gradually settles down to lower values with increased percentage of volume merging between the experimental and theoretical volumes. As expected, the *R*-factor and the $Q^{1/6}$-factor were also found to decrease as the refinement progressed. The structures clearly improved at each refinement step. Both the total energy and the constraint energy cannot be used as criteria for quality of refinement because the error bars and force constants on the restraints were tightened during the molecular dynamics refinement.

For the final iterative cycle, 540 distance restraints were incorporated into the refinement, with 58 of them between hydrocarbon protons and DNA base or sugar protons. A stereoview of the final averaged structure is shown in Figure 5. Structural refinement statistics for the final structure are listed in Table 5. In the final structure, the hydrocarbon remains intercalated in the 5′-direction from the modified A^*_6, and T_{17} is stacked underneath the aromatic portion of

Table 4: MORASS Structure Calculation Progression

iteration[a]	% RMS_{vol}[b]	*R*-factor	$Q^{1/6}$-factor	E_{amber}[c]	E_{const}	force[d]/% error
0	355.4	0.4922	0.1059			
1	103.3	0.3857	0.0800	−6256.9	92.0	5/20
2	96.3	0.3842	0.0768	−6434.7	96.2	5/18
3	78.7	0.3756	0.0747	−6515.7	160.5	5/15
4	82.5	0.3808	0.0751	−6190.6	186.0	7/15
5	79.1	0.3807	0.0748	−6089.0	164.2	7/15
6	83.3	0.3945	0.0771	−6081.3	93.2	7/13
7 (SA)[e]	66.2	0.3622	0.0674	−6147.7		
⟨SA⟩[f]	67.3 ± 1.8	0.3716 ± 0.021	0.0685 ± 0.0018	−6247.1 ± 132.1	64.8 ± 7.0	7(10)[g]/13

[a] MORASS iteration number. [b] The average of the percent RMS differences between the experimental and theoretical volumes. [c] Energy calculated in vacuo. [d] Flatwell potential function parameters [force constant in kcal/(mol Å^2); error is the permitted error on the constraining distances]. [e] Values for the final average structure (SA). [f] ⟨SA⟩ = average values for the 10 final structures. [g] The number in parentheses is the force constant applied to additional restraints derived by estimating NOE strengths from data in H_2O involving exchangeable protons.

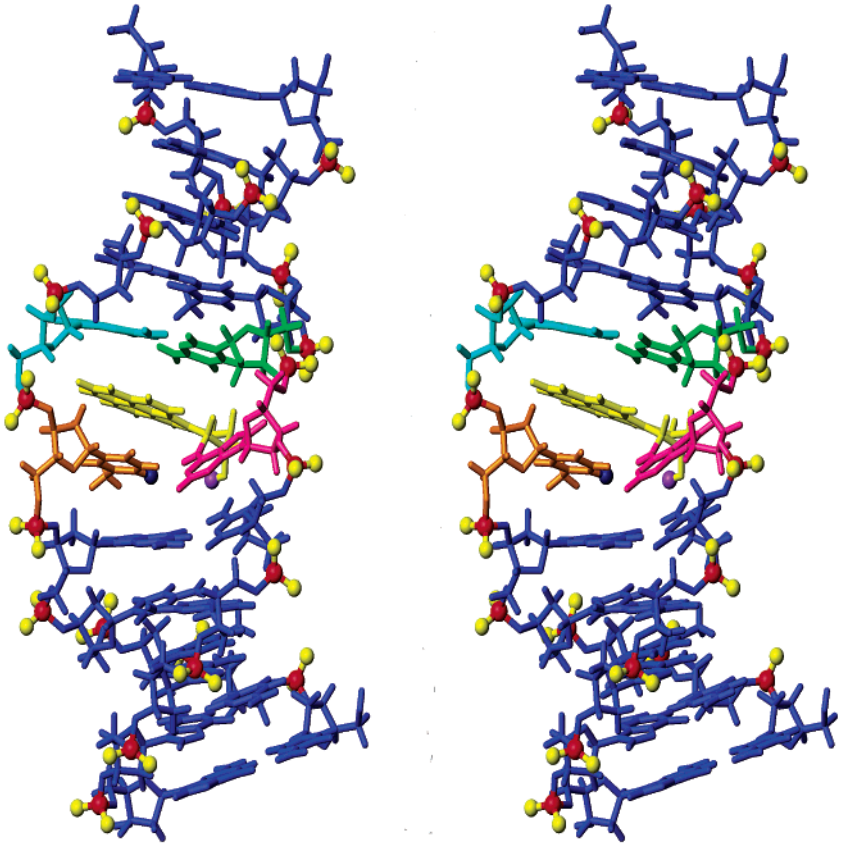

FIGURE 5: Stereoview of the refined MORASS round 6 structure of the 11-mer duplex containing the cis-opened (10*R*)-BP H_4E-dA adduct. The deoxyribose ring and base of the adducted A^*_6 are shown in pink, and the BP system is shown in yellow.

the hydrocarbon. Although no hydrogen bond restraint was used for this base pair in the structure refinements, the hydrogen bond of this base pair remains intact. This agrees with the observation of imino−amino cross-peaks observed in the 2D NOESY spectra collected in H_2O.

Chemical Exchange-Only Spectra: Evidence for a Possible Minor Conformer. In a 150 ms exchange-only spectrum, nine very weak, positive cross-peaks are observed which may correspond to the exchange between two conformers. However, these peaks are approximately the same intensity as several negative peaks that correspond to H2′ to H2″ ROESY peaks. Because this spectrum is a subtraction of NOESY and ROESY interactions, these weak peaks may in fact be the result of slightly imperfect subtraction. Notably, none of these possible exchange cross-peaks involves the adducted base pair A^*_6-T_{17} or its immediate neighbors. One of these positive cross-peaks, from 8.13 (A_{19} H8, major) to 8.53 (minor), appears to be the result of exchange. In the 200 ms D_2O NOESY spectrum, a small diagonal peak at 8.53 ppm was observed that has no NOESY cross-peaks. The other possible minor chemical shifts also do not show any NOE cross-peaks (when resolved enough from other resonances to be determined), even to the chemical shift indicated as its possible major conformation. Another possible exchange peak is between resonances at 7.63 and 7.96 ppm. The resonance at 7.63 ppm corresponds to the H2 proton of either A_{19}, mentioned above, or A_9. Exchange peaks from 5.84 ppm to both 6.36 and 5.29 ppm may correspond with the H1′ protons of T_4, which is across the duplex from A_{19}, and G_3, both of which have H1′ chemical shifts of 5.84 ppm. Residue T_4 is two residues in the 5′-direction from the adducted base A^*_6. It is interesting to note that, in two previous structures

Table 5: Analysis of the MORASS/MD Generated Structures of the (10*R*)-BP H_4E Adduct

NMR Distance Constraints			
total restraints (dihedral restraints)	626 (86)		
interresidue restraints	257		
intraresidue restraints	283		
BP to DNA restraints	58		
Structural Statistics			
MORASS/NMR figures of merit	% RMS_{vol}	*R*-factor	$Q^{1/6}$-factor
final averaged structure	66.2	0.3622	0.0674
ensemble	67.3 ± 1.8	0.3716 ± 0.0206	0.0685 ± 0.0018
RMSD of NOE violations (Å)	0.044 ± 0.117		
no. of NOE violations >0.5 Å	5 ± 2		
no. of NOE violations 0.3−0.5 Å	20 ± 3		
RMSD from ideal geometry			
bond length (Å)	0.0066 ± 0.0001		
bond angle (deg)	4.07 ± 0.06		
pairwise RMSD (Å)			
over all atoms			
final ave. vs starting (intercalated)	1.89		
model			
final ave. vs 10 structures	0.78 ± 0.28		

(*14*, *15*) of BP DE-dA adducts, the residue situated two bases in the 5′-direction of the adduct proved to be the most difficult to assign due to the effects of dynamic line broadening.

Regardless of the validity of the aforementioned tentative assignments of these possible exchange peaks, the population of the minor species is very small. The volume of the minor diagonal peak at 8.53 ppm (volume = 10) versus that of the major diagonal peak at 8.13 ppm (1760) suggests that the population of the minor conformation is less than 1%. This is consistent with a tight structure for the major conformer with little apparent disorder at the adduct site. This conclusion is also supported by the sharp NOESY cross-peaks observed for all of the residues of this duplex. In contrast, an earlier BP DE-dA adduct structure (*15*) exhibited very broad NOESY cross-peaks for the BP moiety and several of the DNA residues as well as well-defined exchange cross-peaks between major and minor conformations, even though the minor population was small (less than 5%).

DISCUSSION

The present (10*R*)-dA adducted duplex consists almost exclusively of a single well-defined conformer. The NOESY cross-peak patterns and the r-MD refined structure show that the hydrocarbon is intercalated from the major groove between the C_5-G_{18} and A^*_6-T_{17} base pairs. The intercalated hydrocarbon extends toward the complementary strand and stacks extensively with the T_{17} and G_{18} residues. All of the residues in the duplex, including A^*_6, have anti glycosidic torsional angles and adopt a B-DNA structure. Furthermore, the base pair at the lesion site remains intact, and the adducted base retains a hydrogen bond with T_{17} in the opposite strand. In all PAH-dA adducts studied so far, the intercalation site of the hydrocarbon is determined by the chirality at the site of attachment to the adenine base. The aromatic moiety is inserted on the 5′-side of the modified adenine in the case of 10*R* adducts and on the 3′-side of the adenine in the case of their 10*S* diastereomers. The present BP H_4E-adducted 11-mer fits this same structural motif, as the hydrocarbon is intercalated on the 5′-side of A^*_6. The plane of the pyrene moiety is nearly perpendicular to the helical axis, allowing effective intercalation (Figure 5).

Table 6: Helical Parameters for the Adducted Base Pair and Its Two Nearest-Neighbor Base Pairs in the Cis BP H_4E and DE-2 Adducted Duplexes[a] Calculated by Curves[b]

	structure		
parameter	cis BP H_4E (MORASS)	cis BP H_4E (ensemble)	cis DE-2
stretch			
C_5-G_{18}	−0.01	−0.02 ± 0.11	−0.20
A^*_6-T_{17}	0.49	0.01 ± 0.07	−0.09
C_7-G_{16}	−0.02	0.00 ± 0.14	−0.10
buckle			
C_5-G_{18}	−0.7	10.4 ± 1.1	39.1
A^*_6-T_{17}	−32.8	−15.2 ± 4.4	−35.2
C_7-G_{16}	−19.5	−4.6 ± 6.5	−11.7
rise			
C_5-G_{18}/A^*_6-T_{17}	7.13	6.98 ± 0.20	8.14
A^*_6-T_{17}/C_7-G_{16}	3.28	3.42 ± 0.30	3.05
tilt			
C_5-G_{18}/A^*_6-T_{17}	−22.4	−20.5 ± 3.2	−22.4
A^*_6-T_{17}/C_7-G_{16}	1.2	0.6 ± 1.5	2.6
twist			
C_5-G_{18}/A^*_6-T_{17}	22.6	12.0 ± 2.6	48.3
A^*_6-T_{17}/C_7-G_{16}	18.4	17.2 ± 2.6	30.8
roll			
C_5-G_{18}/A^*_6-T_{17}	12.9	7.6 ± 5.5	1.82
A^*_6-T_{17}/C_7-G_{16}	−1.3	8.3 ± 3.4	13.9

[a] Values reported for the cis DE-2 adduct are averages determined from analysis of each of the six refined structures (*11*), and those for the BP H_4E (present report) were calculated using our minimized, round 6 MORASS structure (Figure 5) or for the ensemble of 10 final structures (Figure 6). Angles are in degrees and distances are in angstroms. [b] From Curves program (*35*).

Table 7: Selected Sugar−Base and Base−Benzo[*a*]pyrene Bond Angles[a]

structure(s)	χ	α'	β'
minimized average structure	253	158	103
ensemble of 10 structures	256 ± 4	158 ± 9	97 ± 11
cis BP DE-2[b]	258 ± 6	160 ± 10	107 ± 14
low-energy domain III[c]	215 + 70/−40	165 ± 30	100 ± 25

[a] The dihedral bond angles (in degrees) χ, α', and β' are defined as follows: χ = O4′−C1′−N9−C4; α'= N1−C6−N^6−C10(BP); β' = C6−N^6−C10(BP)−C9(BP). [b] From ref *11*. [c] From ref *37*.

Calculated helical parameters (Table 6) and torsional angles (Table 7 and Supporting Information) showed significant deviations around the lesion site. Intercalation of the bulky BP moiety into the helix causes local unwinding of the helix, as evidenced by the lower twist angle between the A^*_6-T_{17} and C_7-G_{16} base pairs (10−18° compared to 34° for canonical B-DNA). Intercalation of the hydrocarbon also causes an increase in the helical rise between the base pairs C_5-G_{18} and A^*_6-T_{17} to ∼7.1 Å, compared to an average value of 3.4 Å observed for the other base pairs in the duplex (not shown). The adducted base A^*_6 retains hydrogen bonding with the complementary T_{17}, although this base pair is markedly buckled. This also causes significant buckling of the C_7-G_{16} base pair.

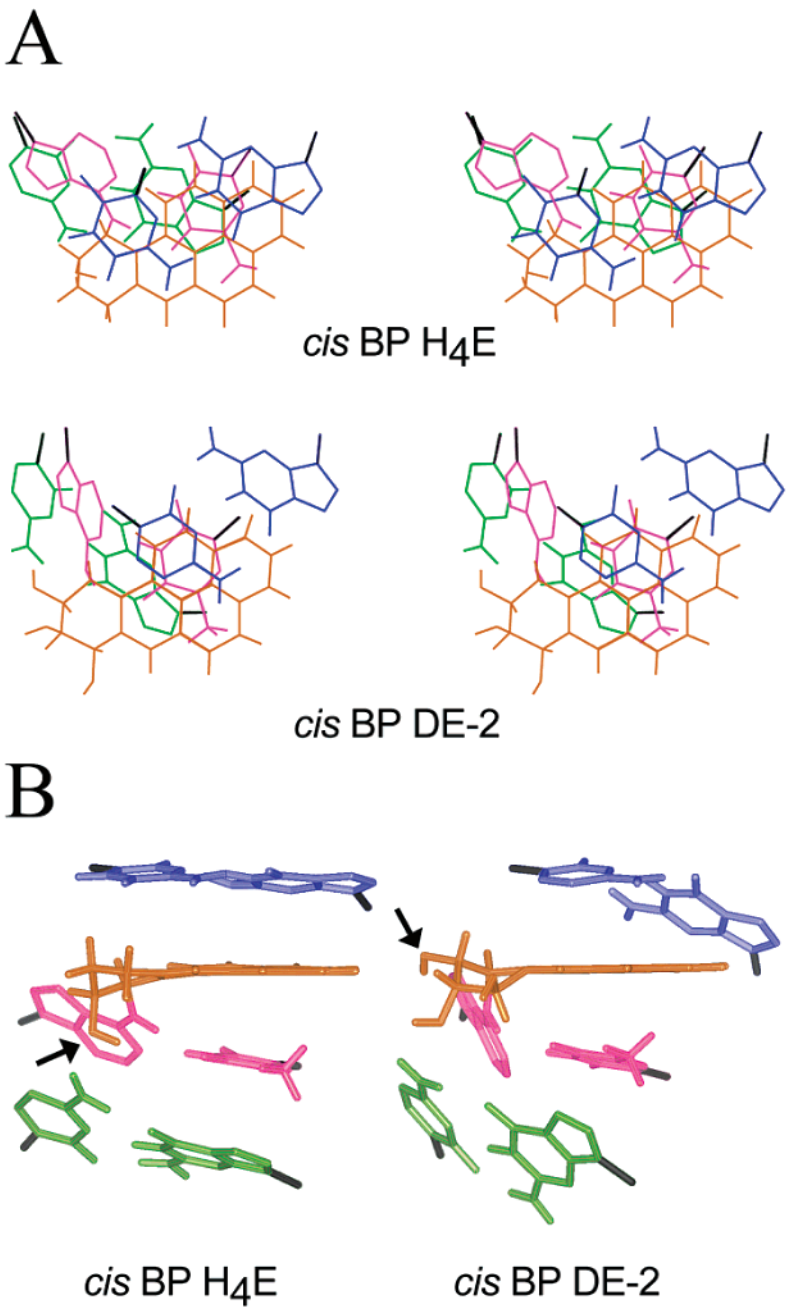

FIGURE 6: (A) Stereoviews of the present cis BP H_4E adduct (energy-minimized average structure) and the previously described (*11*) cis BP DE-2 adduct in an oligonucleotide with the same −CA*C− local sequence, looking down at the plane of the pyrene rings from the 5′-end of the adducted DNA strand. Coordinates for the cis BP DE-2 adducted duplex represent an average of the six structures obtained from the RCSB Protein Data Bank (acquisition number 1AXV). The pyrene ring systems for this structure and the current BP H_4E adduct structure were superimposed and oriented to lie in the plane of the paper. For clarity, only the hydrocarbon moiety (yellow) and the base pairs C_5-G_{18} (blue), A_6-T_{17} (magenta), and C_7-G_{16} (green) are shown. For the hydrocarbon moiety, all hydrogen atoms are shown, but in the representation of the bases, carbon−hydrogen bonds are omitted, so that only hydrogen atoms bonded to nitrogen are shown. The glycosidic bond to each base is shown in black. (B) Nonstereo representation of the same structures rotated 90°, with the C_5-G_{18} base pair at the top. Arrows indicate the C_9-hydroxyl group in each structure.

The hydrocarbon−base and base−deoxyribose torsion angles changed little from the starting structure to the final structure. In the creation of the starting model the deoxyribose−base H1′−C1′−N9−C8 torsion angle was manually changed from −161° to −172° in order to form an intercalated starting structure. In the final structure, this torsion angle is −167°. The dA*$_6$ base−hydrocarbon torsion angle, H6−N^6−C10−H10, changed from 150° in the initial structure to 146.5° in the final structure. This is unsurprising because the torsion angle space that provides an intercalated structure consistent with the NOE data is very limited, as indicated by the small deviations observed for the χ, α', and β' dihedral angles (Table 7).

Effect of the Hydroxyl Groups. Although several NMR structural studies exist for BP DE-adducted DNA duplexes, no structural information on BP H_4E-adducted oligonucleotides has been available prior to the present study. Figure 6 compares the local structure of the oligonucleotide duplex (*11*) containing the cis-opened (10*R*)-BP DE-2 dA adduct (referred to as cis anti) with the present BP H_4E adduct in a sequence (−CA*C−) with the same nearest-neighbor base pairs. Comparison of selected helical parameters for the two

structures (Table 6), calculated by use of the program Curves (*35*), supports the intuitive conclusions based in Figure 6. Calculation of these parameters by a different program, 3DNA (*36*), gave values that were generally in excellent agreement with those shown. With both adducts, the geometry of stacking between T_{17} and the hydrocarbon is similar. Although the modified A^*_6-T_{17} base pair was buckled to about the same extent in the round 6 MORASS structure (−33°) and the BP DE structure (−35°), the buckling in the BP H_4E adduct diminished to $-15 \pm 4°$ for the ensemble of 10 structures determined from the 50 ps r-MD calculation. This change was accompanied by an increase in the positive C_5-G_{18} buckle (−0.7 to 10.4°) and a decrease in the negative buckling angle (−19.5° to $-4.6 \pm 6.5°$) for the C_7-G_{16} base pair. In both structures, there is local distortion of several base pairs flanking the lesion site. The C_7-G_{16} base pair is buckled in both structures to permit base stacking of C_7 with A_6. The observed helical twist between the A^*_6-T_{17} and C_7-G_{16} base pairs is appreciably smaller ($17 \pm 3°$) with the BP H_4E than with the BP DE adduct (31°). The most notable differences between the two structures are in the orientation of the C_5-G_{18} base pair and in the angle between the adducted adenine base and the hydrocarbon. As Figure 6 shows, the planes defined by the hydrocarbon and by the adducted adenine are significantly more tilted relative to each other for the BP DE-adducted duplex than for the BP H_4E adduct. The angles between the adducted base and the pyrene ring system for the present structure and that of the BP DE-2 adducted duplex (*11*), as defined by the angle between the normal vectors for each plane, are 41° and 65°, respectively. Despite this difference, the χ, α', and β' angles of the present BP H_4E are nearly identical to those of the BP DE adduct (*11*), and they fall within the low-energy domain III defined for *cis*-(10*R*)-BP DE dA adducts (*37*) (Table 7). However, the difference in relative plane orientation may be explained by differing ring puckers for the aliphatic portion of the BP systems. In the present structure, the C_9−OH is pseudoaxial and points downward (in the 3′-direction relative to the adducted DNA strand as shown by the arrow in Figure 6B, left). In contrast, the aliphatic ring of the BP DE-2 adduct is puckered such that the C_9−OH is pseudoequatorial (arrow in Figure 6B, right). Conformational differences in the aliphatic rings of BP H_4E relative to BP DEs have previously been proposed (*3*).

Because of the smaller angle between the pyrene ring system and the A^*_6 base in the BP H_4E-adducted duplex, the C_5-G_{18} base pair stacks more favorably with the hydrocarbon and shows less significant buckling (10°), whereas in the DE-adducted duplex it is markedly buckled (39°). Furthermore, the twist angle between the C_5-G_{18} and A^*_6-T_{17} base pairs is appreciably smaller ($12 \pm 3°$) for the BP H_4E relative to the DE adduct (47−48°). A previously reported (*11*) value of 27.2° for this twist angle in the cis BP DE adducted structure, calculated using the program compDNA (*38*), was inconsistent with our values determined by either Curves or 3DNA. We recalculated this parameter using compDNA and obtained a value of 47°, in agreement with our other calculations. This value is also consistent with the appearance of the stacked base pairs as shown in Figure 6A, and we believe it to be correct. As a result of this twist and buckle, the C_5-G_{18} base pair in the DE-adducted structure is displaced relative to the A^*_6-T_{17} base pair (Figure 6A). In contrast, the C_5-G_{18} base pair in the BP H_4E-adducted duplex lies in a plane above and nearly parallel to the hydrocarbon to provide *much more efficient stacking* with G_{18}. The rise between the adducted base pair and the C_5-G_{18} base pair immediately above it is ∼7 Å as compared to ∼8 Å for the DE adduct, possibly due to this more favorable stacking. The tetrahydro ring of the BP H_4E adduct lies under C_5 and is less exposed than that of the DE adduct. The absence of hydroxyl groups at C7 and C8 presumably allows the BP H_4E moiety to insert farther into the helix (Figure 6A). Efficient stacking between the flanking base pairs and the hydrocarbon in the present BP H_4E adduct is consistent with a single, relatively rigid conformation with little fluxional behavior at the adduct site, as shown by the observed narrow NMR line widths. In contrast to the present BP H_4E structure, the 2D NOESY spectra for the (10*R*)-BP DE-2-adducted duplex (*11*) did not show a diagonal cross-peak for the T_{17} imino proton, indicating increased dynamics around the lesion.

The effect of the hydroxyl groups on biological activity is not clear. BP H_4E has been found to be either less or more mutagenic than the DEs, depending on the cells tested (*9*). Distortion of DNA by BP DE adducts has been suggested to increase the susceptibility of these lesions to repair (*39*). Although no studies of DNA repair exist for BP H_4E adducts, it is possible to speculate that the tighter structure and the relatively small distortion of the DNA helix in the present BP H_4E adduct may make it less visible to repair enzymes than the corresponding DE adduct. Thus, such a BP H_4E adduct could persist longer in the cellular environment, with a resultant increase in its mutagenic potential. Site-specific mutagenesis studies (*10*) of BP-dA adducts in an *E. coli*−M13 system have shown that the present cis BP H_4E (10*R*)-dA adduct gives an ∼3-fold greater frequency of mutations (predominantly A → T) than the corresponding cis DE-2 (10*R*)-dA adduct. Since repair of the lesion is not possible with the single-stranded M13 vector, effects on repair cannot explain this result, and the structural basis for enhanced incorrect translesional synthesis past the present adduct in *E. coli* remains to be elucidated.

ACKNOWLEDGMENT

We thank Dr. Victor Zhurkin (National Cancer Institute, NIH) for calculation of the helical parameters using compDNA and Dr. Suse Broyde (New York University) for helpful discussions.

SUPPORTING INFORMATION AVAILABLE

Scheme for the synthesis of the cis BP H_4E dA phosphoramidite, circular dichroism spectra of the purified, single-stranded oligonucleotide 11-mers containing the cis-opened (10*R*)- and (10*S*)-BP H_4E adducts at A^*_6, and a table containing the backbone dihedral angles calculated for the final averaged structure. This material is available free of charge via the Internet at http://pubs.acs.org.

REFERENCES

1. Thakker, D. R., Yagi, H., Levin, W., Wood, A. W., Conney, A. H., and Jerina, D. M. (1985) in *Bioactivation of Foreign Compounds* (Anders, M. W., Ed.) pp 177−242, Academic Press, New York.

2. Whalen, D. L., Ross, A. M., Yagi, H., Karle, J. M., and Jerina, D. M. (1978) *J. Am. Chem. Soc. 100*, 5218−5219.
3. Jerina, D. M., Chadha, A., Cheh, A. M., Schurdak, M. E., Wood, A. W., and Sayer, J. M. (1991) Covalent bonding of bay-region diol epoxides to nucleic acids, in *Biological Reactive Intermediates IV. Molecular and Cellular Effects and Their Impact on Human Health*, pp 533−553, Plenum Press, New York.
4. Kinoshita, T., Lee, H. M., Harvey, R. G., and Jeffery, A. M. (1982) *Carcinogenesis 3*, 255−260.
5. Sayer, J. M., Shah, J. H., Liang, C., Xie, G., Kroth, H., Yagi, H., Liu, X., Yeh, H. J. C., and Jerina, D. M. (1999) *Polycyclic Aromat. Compd. 17*, 95−104.
6. Panthananickal, A., Weller, P., and Marnett, L. J. (1983) *J. Biol. Chem. 258*, 4411−4418.
7. Chiu, P. L., and Yang, S. K. (1986) *Cancer Res. 46*, 5084−5094.
8. Adams, J. D., Jr., Yagi, H., Levin, W., and Jerina, D. M. (1995) *Chem.-Biol. Interact. 5*, 57−77.
9. Wood, A. W., Wislocki, P. G., Chang, R. L., Levin, W., Lu, A. Y. H., Yagi, H., Hernandez, O., Jerina, D. A., and Conney, A. H. (1976) *Cancer Res. 36*, 3358−3366.
10. Ramos, L. A., Sayer, J. M., Yagi, H., Shah, J. H., Dipple, A., and Jerina, D. M. (2001) *Chem. Res. Toxicol. 14*, 1082−1089.
11. Mao, B., Gu, Z., Gorin, A., Chen, J., Hingerty, B. E., Amin, S., Broyde, S., Geacintov, N. E., and Patel, D. J. (1999) *Biochemistry 38*, 10831−10842.
12. Schurter, E. J., Sayer, J. M., Oh-hara, T., Yeh, H. J. C., Yagi, H., Luxon, B. A., Jerina, D. M., and Gorenstein, D. G. (1995) *Biochemistry 34*, 9009−9020.
13. Zegar, I. S., Kim, S. J., Johansen, T. N., Horton, P. J., Harris, C. M., Harris, T. M., and Stone, M. P. (1996) *Biochemistry 35*, 6212−6224.
14. Zegar, I. S., Chary, P., Jabil, R. J., Tamura, P. J., Johansen, T. N., Lloyd, R. S., Harris, C. M., Harris, T. M., and Stone, M. P. (1998) *Biochemistry 37*, 16515−16528.
15. Volk, D. E., Rice, J. S., Luxon, B. A., Yeh, H. J. C., Liang, C., Xie, G., Sayer, J. M., Jerina, D. M., and Gorenstein, D. G. (2000) *Biochemistry 39*, 14040−14053.
16. Pradhan, P., Lu, X., Shah, J. H., Sayer, J. M., Jerina, D. M., and Yeh, H. J. C. (2003) manuscript in preparation.
17. Lakshman, M. K., Sayer, J. M., Yagi, H., and Jerina, D. M. (1992) *J. Org. Chem. 57*, 4585−4590.
18. Custer, L., Zajc, B., Sayer, J. M., Cullinane, C., Phillips, D. R., Cheh, A. M., Jerina, D. M., Bohr, V. A., and Mazur, S. J. (1999) *Biochemistry 38*, 569−581.
19. Christner, D. F., Lakshman, M. K., Sayer, J. M., Jerina, D. M., and Dipple, A. (1994) *Biochemistry 33*, 14297−14305.
20. Schurter, E. J., Yeh, H. J. C., Sayer, J., Lakshman, M. K., Yagi, H., Jerina, D. M., and Gorenstein, D. G. (1995) *Biochemistry 34*, 1364−1375.
21. Smallcombe, S. H., Patt, S. L., and Keifer, P. A. (1995) *J. Magn. Reson. 117*, 295−303.
22. Rance, M. (1987) *J. Magn. Reson. 74*, 557−564.
23. Bax, A., and Davis, D. G. (1985) *J. Magn. Reson. 63*, 207−213.
24. Macura, S., Westler, W. M., and Markley, J. L. (1994) Two-dimensional exchange spectroscopy of proteins, in *Methods in Enzymology*, Vol. 239, pp 106−144, Academic Press, San Diego.
25. Frisch, M. J., Trucks, G. W., Schlegel, H. B., Gill, P. M. W., Johnson, B. G., Robb, M. A., Cheeseman, J. R., Keith, T., Petersson, G. A., Montgomery, J. A., Raghavachari, K., Al-Laham, M. A., Zakrzewski, V. G., Ortiz, J. V., Foresman, J. B., Cioslowski, J., Stefanov, B. B., Nanayakkara, A., Challacombe, M., Peng, C. Y., Ayala, P. Y., Chen, W., Wong, M. W., Andres, J. L., Replogle, E. S., Gomperts, R., Martin, R. L., Fox, D. J., Binkley, J. S., Defrees, D. J., Baker, J., Stewart, J. P., Head-Gordon, M., Gonzalez, C., and Pople, J. A. (1995) *Gaussian 94, Revision E.4*, Gaussian, Inc., Pittsburgh, PA.
26. Macke, T., and Case, D. A. (2000) *NAB-4.4*, The Scripps Research Institute, San Diego, CA.
27. Case, D. A., Pearlman, D. A., Caldwell, J. W., Cheatham, T. E., Ross, W. S., Simmerling, C. L., Darden, T. A., Merz, K. M., Stanton, R. V., Cheng, A. L., Vincent, J. J., Crowley, M., Ferguson, D. M., Radmer, R. J., Seibel, G. L., Singh, U. C., Weiner, P. K., and Kollman, P. A. (1997) *AMBER 5.0*, University of California, San Francisco.
28. Jorgensen, W. L., Chandrasekkar, J., and Madura, J. D. J. (1983) *J. Chem. Phys. 79*, 926−935.
29. Essmann, U., Perera, L., Berkowitz, M. L., Darden, T., Lee, H., and Pedersen, G. (1995) *J. Chem. Phys. 103*, 8577−8593.
30. Meadows, R., Post, C. B., Luxon, B. A., and Gorenstein, D. G. (1996) *MORASS Program*, University of Texas Medical Branch, Galveston, TX.
31. Ross, W. S. (1994) *CARNAL*, University of California, San Francisco.
32. Schafmeister, C. E. A. F., Ross, W. S., and Romanovski, V. (1995) *LEaP*, University of California, San Francisco.
33. Ferrin, T. E., Huang, C. C., Jarvis, L. C., and Langridge, R. (1988) *J. Mol. Graphics 6*, 13−27.
34. Wuthrich, K. (1986) *NMR of Proteins and Nucleic Acids*, John Wiley and Sons, New York.
35. Lavery, R., and Sklenar, H. J. (1988) *J. Biomol. Struct. Dyn. 6*, 63−91.
36. Lu, X., Shakked, Z., and Olson, W. K. (2000) *J. Mol. Biol. 300*, 819−840.
37. Tan, J., Geacintov, N. E., and Broyde, S. (2000) *Chem. Res. Toxicol. 13*, 811−822.
38. Gorin, A., Zhurkin, V., and Olson, W. (1995) *J. Mol. Biol. 247*, 34−48.
39. Zou, Y., Liu, T.-M., Geacintov, N. E., and Van Houten, B. (1995) *Biochemistry 34*, 13582−13593.

BI026745U